Medical Research Archives

European Society of Medicine

OPEN ACCESS

Published: March 31, 2024

Citation: Bogni, A., et al., 2024. Analysis of TiO2 nanoparticles accumulation *in vitro*. Medical Research Archives, [online] 12(3). https://doi.org/10.18103/mra.v12i3.5272

DOI: https://doi.org/10.18103/mra.v12i3.5272

ISSN: 2375-1924

RESEARCH ARTICLE

Analysis of TiO_2 nanoparticles accumulation *in vitro*

Alessia Bogni[1], Jessica Ponti[1], Uwe Holzwart[1], Agapios Sachinidis[2] and Susanne Bremer-Hoffmann[1*]

[1]European Commission, Joint Research Centre (JRC), Ispra, Italy
[2]University of Cologne, Center of Physiology and Pathophysiology, Institute of Neurophysiology, Cologne, Germany

*susanne.bremer-hoffmann@ec.europa.eu

ABSTRACT

The physicochemical properties of titanium dioxide (TiO_2) in nanoforms is often exploited as colorant in food, pharmaceuticals and other consumer products. However, the current evidence of potential hazards associated with titanium dioxide (TiO_2) in nanoforms led to a ban of TiO_2 as food additive in Europe. This regulatory decision has also an impact on thousands of pharmaceuticals.

In the present study, we tested the internalisation, accumulation and resulting biological effects of different types of TiO_2 nanomaterial in short and long-term vitro cultures. Even if we could demonstrate that all tested cell lines were able to take up and accumulate nanomaterial for a period of up to 30 days, the cellular responses using conventional *in vitro* tests were limited in all tested cell lines. Nevertheless, a transcriptomics study revealed that that the response to the accumulated material differed between two selected cell types. A keratinocyte like cell line reacted with a modified rate of keratinogenesis whereas the enterocyte like cell demonstrated mainly interactions with cell homeostasis. To further clarify possible harmful effects of TiO_2, the study suggests analyzing cell/tissue type specific effects of TiO_2.

Keywords: TiO_2 nanoparticle; accumulation; radioactivity; transcriptomics; Caco-2; HaCaT; Balb/3T3 cells.

1. Introduction

The physicochemical properties of titanium dioxide (TiO_2) in nanoforms have been exploited in many consumer products including cosmetics, e.g as whitener in toothpastes or as UV filter in sunscreens. The food additive "E171" contains about 50% of particles in the nano range and is mainly used as colorant in several nutritional products but also in pharmaceuticals[1]. With a production volume of more than 1000 tons/year and more than 200 entries in the registry for the Registration, Evaluation, Authorisation of Chemicals (REACH), TiO_2 appeared as one of the most manufactured nanomaterials[2] .

In recent years, growing concerns about the potential harmful effects related to TiO_2 in consumer products, led to several regulatory actions in Europe. Based on the observation that deposited particles could be responsible for toxicity and tumor formation in the lung, the Committee for Risk Assessment (RAC) from the European Chemicals Agency (ECHA) proposed in 2019 to classify TiO_2 as a suspected carcinogen if inhaled and the substance or mixture contains more than 1% TiO_2 particles with an aerodynamic diameter ≤10 µm[3]. In 2021, the European Food Safety Agency's (EFSA) panel on Food Additives and Flavorings (FAF) concluded that the food additive E171 can accumulate in the body and potentially induce toxicological effects including immunological reactions, genotoxic effects and neurotoxicity. In addition, the observation that aberrant foci were induced in the intestine of experimental animals was an indication of a possible carcinogenic hazard of the material[1]. The uncertainty related to the safe use of TiO_2 in food led to the ban as a food additive in the EU in 2022 and, additionally, raised concerns about its use in other sectors. The European Medicines Agency (EMA) concluded in its impact assessment that several thousand pharmaceuticals could be affected[4] by the regulation of TiO_2. According to trade associations, around 91,000 human medicinal products and 800 veterinary medicinal products mainly used for oral administration, contain TiO_2 as an opacifier and colorant. In the light of these decisions, in 2022 the European Commission requested a scientific opinion also on the safety of TiO_2 used in cosmetic products[5]. The case of TiO_2, a nanomaterial that is used in a wide range of consumer product types, illustrates the need to align hazard assessment across the various European scientific committees and agencies as envisaged in the one substance-one assessment action of the chemical strategy for sustainability (CSS)[6]. Whereas in Europe the uncertainties about the biological effects were considered as safety concern, other regions such as the UK, came to a different conclusion[7]. In order to support a harmonized regulation of TiO_2 in various regions, the existing knowledge gaps including dose-response relationships, mechanisms of toxicity and (long-term) effects of different exposure routes need to be addressed.

TiO_2 nanoparticles have a low oral systemic bioavailability *in vivo* but, once taken up have a biological half-life of several years[8–10], demonstrating a potential for accumulation. The particles can be taken up e.g. from the small intestine by the paracellular pathway, by endocytosis and into M-cells of the Peyer's patches[11,12] however, potential local gastrointestinal effects on the gut mucosa, the

intestinal barrier and immunological systems are not well understood[13]. New approach methodologies (NAMs) including in-vitro tests can be instrumental in filling knowledge gaps and explaining the potential modes of action (MoA) of TiO_2 resulting from its various physico-chemical characteristics. Consequently, the choice of the *in vitro* model is crucial and will strongly depend on the toxicological question. The availability of a toolbox with well-characterized, reliable and relevant biological models would be instrumental in obtaining quick answers to key questions about the effects of substances such as TiO_2.

In this study, we investigated the capability of different potential target cell models to internalize and accumulate three forms of TiO_2 used as representative examples of materials for healthcare and food products. Different monocultures of keratinocyte like cells (HaCaT), enterocyte like cells (Caco-2) as well as the murine fibroblast Balb/3T3 cell line were exposed to TiO_2 and demonstrated their capability to take up and accumulate TiO_2 in long-term cell cultures by using not only microscopical techniques but also radiotracer. In order to establish a hypothesis on potential perturbations of physiological pathways triggered by the accumulation of nanomaterial, we performed a transcriptomic analysis[14].

2. Material and Methods

2.1. TIO_2 NPS DISPERSION AND CHARACTERISATION

NM104 (JRCNM62002, rutile, coated Nanoparticles), and NM105 (JRCNM01005, rutile-anatase, uncoated Nanoparticles) were supplied by the Joint Research Centre Nanomaterials Repository as powder samples representative of industrially manufactured nanomaterials. A report containing a complete physico-chemical characterization of the pristine NM104 and NM105 materials was previously published (EUR 26637 EN). The E171 food grade TiO_2, corresponds to the pristine material Candies B as reported by Geiss et al 2020[15].

NM104, NM105 and E171 materials were dispersed in Milli-Q water to produce final concentrations of 1.39mg/mL, 1.39mg/mL and 1.5 mg/mL respectively. The suspensions were sonicated for 30 minutes with a S3 probe sonicator (Branson 200), 70% power, 0.5 amplitude, in an ice container, before being put in an ultrasonic water bath for 30 minutes. Before starting with the treatment of cell cultures, the TiO_2 NPs suspensions were sonicated again in the water bath for 15 minutes. The NPs were tested for the presence of endotoxin using Chromo-LAL test (Associates of Cape Cod Europe GmbH, Germany), resulting in a very low presence of endotoxin (<0.005 EU/mL).

The proton irradiation of the TiO_2 nanoparticles was performed on batches of 27 mg of NM104 NPs and resulted in an activity concentration of 6.56 MBq/mg for the NM104 NPs at the end of bombardment and of 6.27 MBq/mg for the NM010a at the end of bombardment. The characteristics of irradiated nanoparticle were analysed (see supplements).

2.2 CELL CULTURE

Human keratinocyte cells (HaCaT) were originally supplied by the German Cancer Research Center (Germany), human intestinal epithelial cells (Caco-2) were originally purchased from the American Type Culture

Collection (ATCC). Balb/3T3 mouse fibroblasts stemming from the clone A31-1-1 were purchased from Hatano Research Institute (Japan).

HaCaT were cultured in DMEM high glucose (Invitrogen, Italy) with 10% (v/v) Fetal Clone II serum (Hyclone, Celbio, Italy), 4mM l-glutamine (Invitrogen, Italy) and 1% (v/v) pen/strep (Invitrogen, Italy). Caco-2 were cultured in DMEM high glucose (Invitrogen, Italy) added with 10% (v/v) FBS North America Origin and 4mM L-glutamine (Invitrogen, Italy) and 1% (v/v) pen/strep (Invitrogen, Italy). Balb/3T3 were cultured in Minimum Essential Medium (MEM) low glucose added with 10% (v/v) Fetal Bovine Serum (FBS) and 0.6% (v/v) pen/strep (Invitrogen, Italy). All cell cultures were maintained in standard cell culture conditions (37◦C, 5% CO2 and 95% humidity, Heraeus incubator, Germany). Cells were cultivated up to 70–80% confluence in tissue culture-treated flasks (BD Falcon; Milan, Italy) and passaged twice a week.

2.3. TiO_2 NPs exposure schemes for internalisation, accumulation and cellular effects Balb/3T3, Caco-2 and HaCaT cells were seeded in Petri dishes on D0 at a density of 250000 cells/dish in 5 mL of complete medium, in order to obtain a cell monolayer at maximum 3 days in culture.

Three different treatment protocols (Fig 1A-C) were developed in order to assess the internalisation, accumulation and resulting biological effects of TiO_2 after single and repeated dose exposures. In long-term cell cultures (up to 5 weeks) biological effects of the internalized and accumulated particles were investigated. Since the dose range finding studies did not demonstrate any statistical significant cytotoxicity by using the one way Anova test (see supplements), we exposed the cells to a TiO_2 concentration of 100µg/mL which is the highest dose as recommended in the OECD guidance document for genotoxicity[16].

In the exposure protocol 1, Balb/3T3 were seeded and after 24 hours were to exposed a TiO_2 suspension with a final concentration of 100µg/mL (Fig1A). After 3 days of exposure, the TiO_2 suspension was removed and replaced with fresh culture medium. Cells were kept in culture up to 28-31 days. The exposure protocol 1 was used to assess the following biological parameters: i) potential cytotoxic effects by using the Colony forming assay (CFE) and by measuring viable cells using flow cytometry; ii) morphological changes of Balb/3T3 cells using the cell transformation assay (CTA), iii) cellular uptake and accumulation of TiO_2 by using transmission electron microscopy (TEM), vi) γ-ray spectrometry to quantify the accumulation of radioactive labelled TiO_2 particles and v) barrier integrity of the nanoparticles using cell impedance measurements (ECIS).

The second exposure protocol (Fig.1B) was designed to simulate a repeated dose scenario. As previously, TiO_2 was also added to the cell culture 24h after seeding but in the exposure protocol, the TiO_2 suspension was replaced after 24h, 48h and 72h after starting the initial exposure. In addition to the described biological endpoints in exposure protocol 1, a transcriptomics study analysing modifications in the gene expression was also performed.

Finally, we quantified the amount of TiO_2 nanoparticles by using radiolabelled $^{[48V]}TiO_2$

NP exposing the cells as described below in protocol 3 (Fig. 1C). The cells were seeded on Day 0 at different concentrations depending on the exposure time foreseen: for the 4h and 24h exposure time, the initial seeding density was 500,000 cells /dish, and for the 72h exposure time 250,000 cells/dish in 100mm dish, both in 5 mL of complete medium. On Day 1, the cells were exposed to 100 µg/mL radiolabelled $^{[48V]}TiO_2$ NP in a total of 4 mL culture medium. After 4h, 24h and 72h, cells were washed twice with PBS and detached with trypsin. Cells were collected and suspended in 5 mL of medium, and the radioactivity was measured. Afterwards, the cells were counted in a Burker cell counting chamber to evaluate the total cell number to be correlated to the residual radioactivity. Each experiment was performed in three technical replicates. All the radioactivity measurements of 48V were performed in 100mm Petri dishes (3 technical replicates), to maintain the same geometry during the analysis in the same detector. The absolute activities of the stock solutions and all specimens derived from the cell culture studies were determined by g-ray spectrometry, using high purity germanium (HPGe) detectors from CANBERRA (USA) and EG&G Ortec (USA). On Day 1, 24 h after the seeding, the medium was replaced with fresh medium containing $^{[48V]}TiO_2$ NP suspensions at a concentration of 100 µg/mL, in a total of 5 mL volume (TiO_2 total is 500µg). The radioactivity of the entire Petri dish (PD) was measured (t=0). On the subsequent days of exposure, i.e. at days 4, 7, 10, 14 and 18, the radioactivity content of the following components was measured: (a) 5mL of medium previously removed from the dish and (b) dish without medium but with attached cells previously exposed. Then, the medium containing 100 µg/mL of $^{[48V]}TiO_2$ NP in suspensions (PD) was added again to the cells. Whenever the culture medium was changed, the radioactivity was re-quantified in the medium removed from the cells and in the empty dish containing cells. This was repeated at every change of medium, twice a week until the end of the treatment at day 20 in technical replicates.

Figure 1. A Exposure protocol 1.

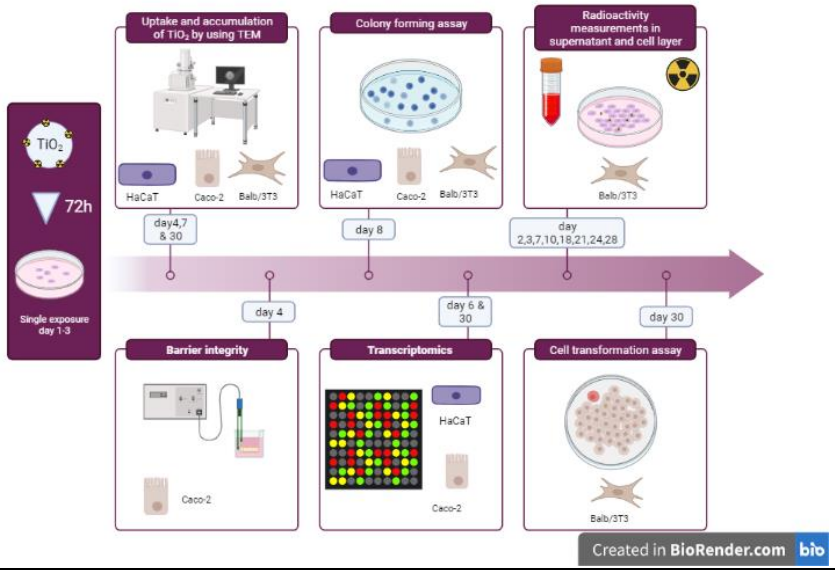

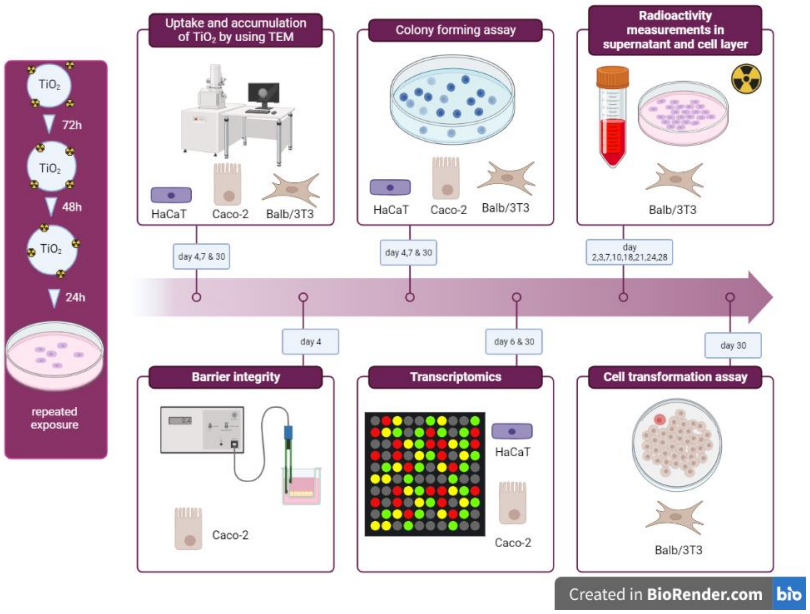

Figure 1. C Exposure protocol 3.

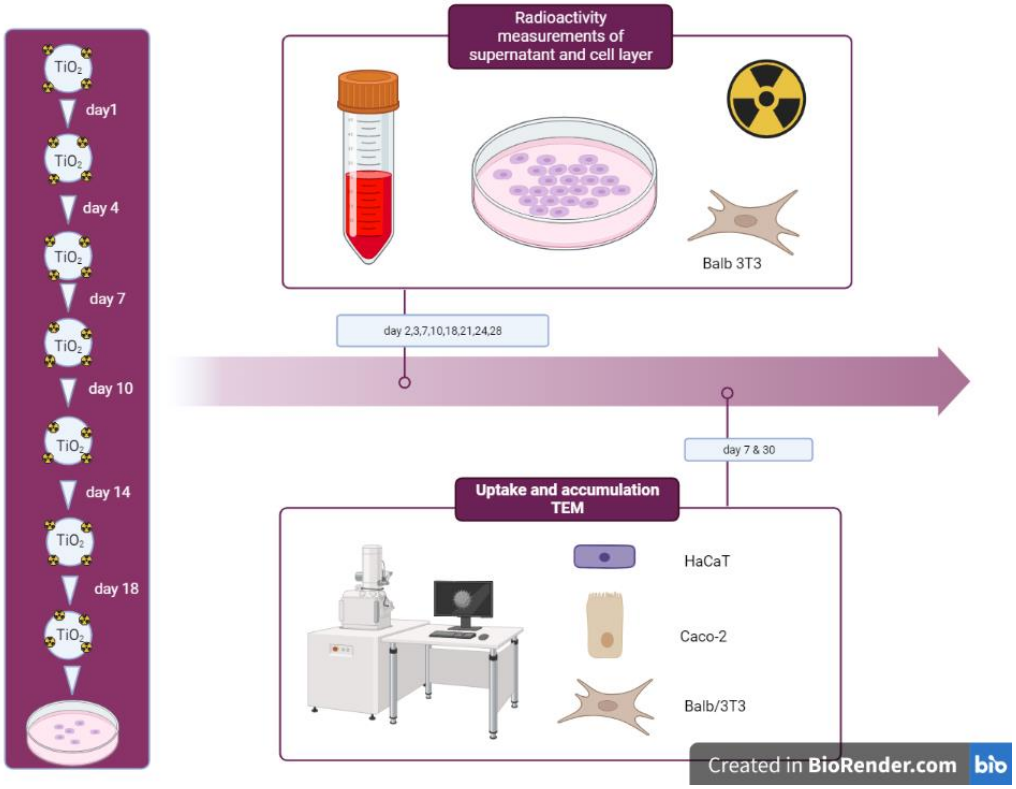

2.4. TRANSMISSION ELECTRON MICROSCOPY

Cells were detached with trypsin, harvested in complete cell culture medium and washed twice with PBS before being fixed in 2% Karnovsky fixative overnight at 4°C. Then, the cells were washed 3 times with 0.05M cacodilate at pH 7.3 and post-fixed in osmium tetroxide solution in 0.1M cacodilate (pH 7.3) for 1h. After 3 washes in cacodilate 0.05M of 10min each, cells were dehydrated in a graded series of ethanol solutions in Milli-Q

water (30%-50%-75%-95% for 15 min each, and 100% for 30 min), incubated in absolute propylene oxide for 20 min (2 changes of 10 min each) and embedded in a solution of 1:1 epoxy resin and propylene oxide for 90 min. This mixture was renewed with pure epoxy resin over night at room temperature and later polymerized at 60°C for 48h. Ultrathin sections (50-70nm) were obtained using Leica EM UC7 ultramicrotome (Leica, Italy) and stained for 25 min with uranyl acetate solution 5% and Reynolds' lead citrate solution for 20 min, washed and dried. All reagents used to prepare solutions, if not specified differently, were supplied by Sigma Aldrich, Italy. The sections were collected on Formvar Carbon coated 200 mesh copper grids (Agar Scientific, USA) and imaged by JEOL JEM-2100 HR-transmission electron microscope at 120kV (JEOL, Italy). At least 20 cells/treatment were qualitatively analysed.

2.5.1. TRANSCRIPTOMICS

The transcriptome analysis study was performed according to the protocol as described by Forcella et al (2020)[17]. In summary, the total RNA was isolated from cells by using RNeasy Plus kit (Qiagen, Milan, Italy). After RNA quantification with a ND-1000 UV–vis spectrophotometer (Thermo Scientific, Wilmington, DE, USA), an Agilent 2100 Bioanalyzer (Agilent Technologies) was used to determine the RNA integrity (RNA integrity Number (RIN) of the samples (all RIN above 9.0). The experiments were performed in three biological replicates. Labelling, (One Color Quick Amp Labelling; Agilent Technologies Inc.) and hybridisation, (Gene Expression Hybridization Kit (Agilent Technologies/ SurePrint G3 Human Gene Expression v2 Microarray/Agilent) were performed according to the instructions of the dedicated kits. After hybridization, the microarray slides were washed and then scanned with an Agilent G2565BA Microarray Scanner (Agilent Technologies Inc.). The scanned images were further processed by using the Agilent Feature Extraction Software (version 10.7.3.1). The green channel was read from the scanned images using the read.images function of the limma package (version 3.34.9) in the R software (version 3.4.2). The signal from each experiment was background corrected using the normexp method with an offset of 20. For each cell type (i.e HaCaT and Caco-2 cells) and time-point (i.e 72 hrs and 5 weeks), a normalization between arrays was performed using the quantile method. The signals from the replicated probes were averaged for each gene using the avereps function and embedded into an ExpressionSet object. After filtering the object for genes with a standard deviation of zero, the genes were submitted to a limma t-test with the standard error of the statistical test being moderated across genes using a Bayesian model from limma (version 3.34.9). The limma t-test was performed by applying a simple contrast model to compare TiO_2 treated and untreated cells. The process was repeated for each cell type and time-point. Gene ontology (GO) terms and KEGG/Reactome pathways deregulated by the nanoparticles were identified by the Metascape bioinformatics tool (https://metascape.org/gp/index.html#/main/step1) as previously described[18].

2.5.2. qPCR VALIDATION OF TRANSCRIPTOMICS DATA

A subset of significantly regulated genes as identified in the transcriptomic study (FGF12,

NAP1L5, SLC28A2, LCE2B, LCE1B) was validated by using real-time RT-PCR (qPCR). The total RNA was isolated using a QIAGEN (Milan, Italy) RNeasy kit. The total RNA was reverse-transcribed using SuperScript II RT (Invitrogen, Carlsbad, CA, USA), oligo dT and random primers, according to the manufacturer's protocol. Each sample was normalized using β-actin gene as internal reference control. The relative expression level was calculated with the Livak method (2[-ΔΔC(T)]) and expressed as a relative fold change between treated and untreated cells. For quantitative real-time PCR, the specific TaqMan probes were used (Hs00912823_m1, Hs00288069_s1, Hs01035846_m1, Hs04194422_s1, Hs00866755_s1).

3. Results

The different forms of TiO_2 particles (NM104, NM105 and E171) were resuspended in complete culture medium and characterised by using dynamic light scattering (DLS), atomic force microscopy (AFM) and atomic absorption spectroscopy (AAS). The obtained data indicated no significant changes in comparison to the characterisation of the pristine material. The data of the characterisation are summarized in the supplements 7.

3.1. Internalisation of TiO_2

In order to demonstrate the capability of the different cell lines to internalise the various forms of TiO_2, we exposed proliferating cells of the various cell lines for 72h. Independently from the applied exposure protocol, we observed TiO_2 uptake in each cell line and for each tested nanomaterial. Figure 2 shows the undamaged cellular ultrastructure in control and exposed cells. TiO_2 nanoparticles were internalised inside endosomes, suggesting the uptake of the nanomaterial through the endo-phagocytosis pathway.

Figure 2. Internalisation of nanomaterial

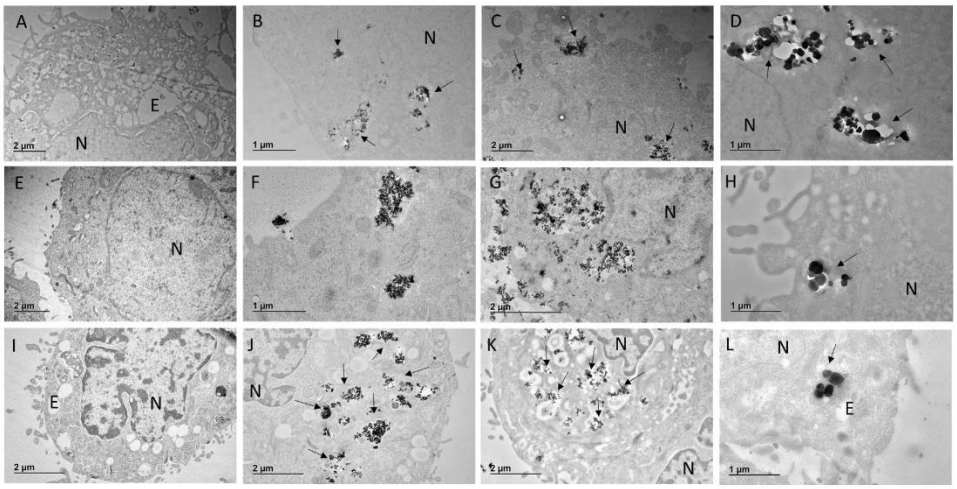

The figure shows the internalisation of nanoparticles after 72 hours exposure to NM104, NM105 or E171. 20-30 cells were investigated for their internalization of TiO_2: Caco-2 cells (A=negative control, B=NM104 exposure, C=NM105 exposure, D=E171 exposure); Balb/3T3 cells (E=negative control, F=NM104 exposure, G=NM105 exposure, H=E171 exposure); HaCaT cells (I=negative control, J=NM104 exposure, K=NM105 exposure, L=E171 exposure). N=nucleus, E=Endosome, arrow=TiO_2 nanoparticles.

3.2. ACCUMULATION OF TIO_2 IN DIFFERENT CELL LINES

The TEM analysis showed that the three selected cell lines Balb/3T3, Caco-2 and HaCaT, were able to take up the various forms of TiO_2 after a repeated exposure to 100 µg/mL TiO_2 (exposure protocol B). It was remarkable that the accumulation of nanomaterial was already visible in phase contrast microscopy. This observation triggered our interest to investigate the accumulation potential of TiO_2 systematically. We could demonstrate that after more than 4 weeks, TiO_2 was still detectable in all investigated cell lines even if the cell treatments of cells were finalised after 72h (Fig 3).

Figure 3. Accumulation of TiO_2 in long-term cell cultures.

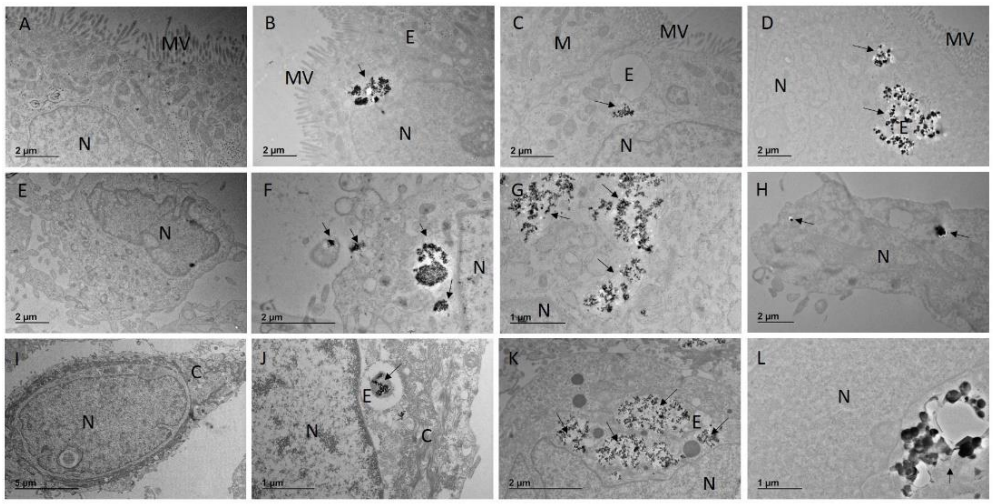

Long-term culture of cells exposed to NM104, NM105 or E171. Caco-2 cells (A=negative control, B=NM104 exposure, C=NM105 exposure, D=E171 exposure); Balb/3T3 cells (E=negative control, F=NM104 exposure, G=NM105 exposure, H=E171 exposure); HaCaT cells (I=negative control, J=NM104 exposure, K=NM105 exposure, L=E171 exposure). N=nucleus, MV=microvilli, E=Endosome, M=mitochondria, C=collagen fibers, arrow=TiO_2 nanoparticles. At least 20 cells were investigated for their accumulation of TiO_2. All cells demonstrated the uptake and accumulation of TiO_2.

3.3. ACCUMULATION STUDIES USING RADIOLABELLED TIO_2 NPS

In order to confirm and quantify the accumulated TiO_2, we exposed Balb/3T3 cells to radioactive labelled NM104-$^{[48V]}TiO_2$ and NM105-$^{[48V]}TiO_2$ following the exposure protocols A-C (Fig 1). The labelling procedure did not affect the investigated physico-chemical properties (see supplements). We could demonstrate that the repeated exposure led to an increased uptake of radioactive material in the monolayer, which largely remained in the cells for 25 days (Fig 4). Table 1 shows the total amount of accumulated material per cells ranging from 13.1 ± 3.5 pg/cell (single exposure) to 100.4 ± 18.1 pg/cell (repeated exposures). Even if repeated dosing resulted in a higher uptake of NM105 and NM104 in cells, the specific type of TiO_2 did not appear to influence the uptake in any of exposure scenarios were observed.

Figure 4. Accumulation of NM104-$^{[48V]}TiO_2$ (A) and NM105-$^{[48V]}TiO_2$ (B) in Balb/3T3 cells .

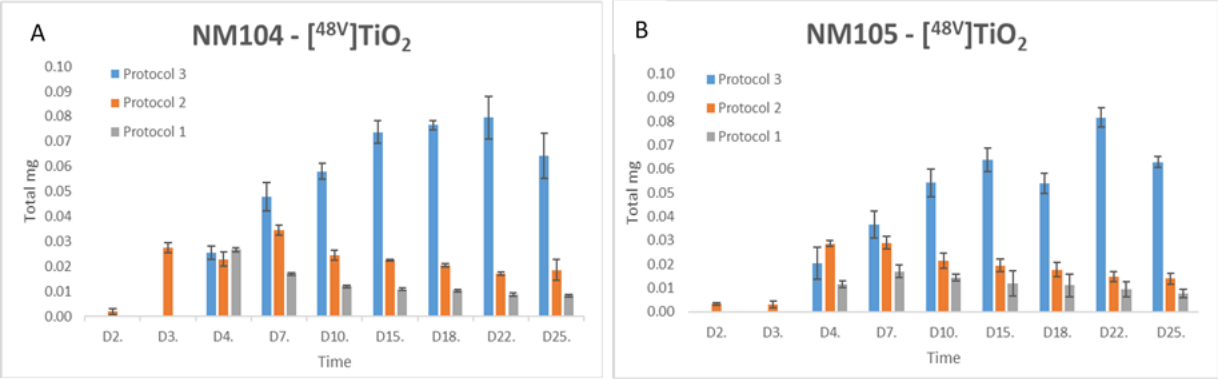

A Monolayer of Balb/3T3 was exposed to radiolabelled TiO_2 NPs according to the protocols 1-3 (Fig 2). The graph shows the total milligrams of TiO_2 accumulated in the entire monolayer of cells (s.d. of 3 technical replicates). The repeated exposure led to higher accumulation rates in the cell independent of the material.

Table 1. Summary of the uptake of labelled nanomaterial uptake in pg/cell.

	Uptake after 28 days in culture (pg/cell)		
	protocol #1	protocol #2	protocol #3
xposure time	72h (single exposure)	24h x 3 (repeated exposure)	72h x 6 (repeated exposure)
NM105	13.1±3.5	23.1 ±3.9	100.4 ±18.1
NM104	15.0 ±2.1	35.1± 3.4	86.7 ±14.1

After finalization of experiments cells of the 3 technical replicates were isolated and the uptake of the nanomaterial/ cell were calculated.

3.4. CELLULAR EFFECTS OF TIO_2 NPS

In order to analyse the effects of the internalised particles, we have performed a battery of in-vitro tests that could point to cellular effects of TiO_2. However, we could not detect an effect on the cell viability of Balb/3T3, Caco-2 and HaCaT cells, as measured in the colony-forming assay and by using flow cytometry (see supplements). Cytotoxicity was also not induced by exposing HaCaT cells treated with NM104 (see supplements). The cell transformation assay did not indicate any morphological changes in treated Balb/3T3 cells (see supplements). In addition, we also measured to which extent E171 can damage the barrier permeability of Caco-2 cells. The experiments performed did not show any decrease in the transendothelial electrical resistance (TEER). However, the TEM analysis of HaCaT cells that were exposed to NM104 demonstrated an increased production of collagen (Fig.5).

Figure 5. Increased production of collagen in long-term cultures of HaCaT

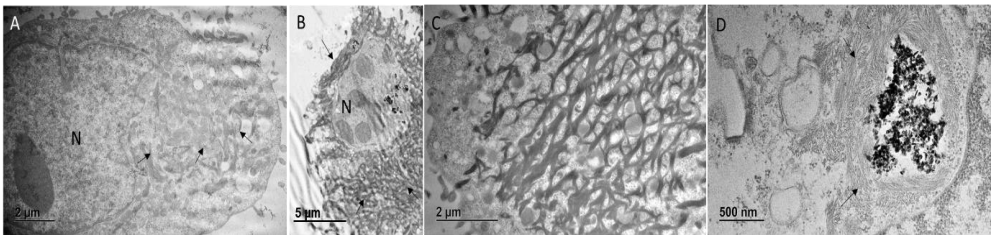

Representative electron microscopy images of unexposed HaCaT cell maintained in culture for 31 days (A) and exposed to NM104 for 72h (exposure protocol see Fig 1B). The pictures B,C,D show a hyper-production of collagen (arrows) largely distributed in the cytoplasm, around the nucleus' perimeter or around endosomes containing nanomaterial (D); N=Nucleus. At least 20 cells were investigated.

3.5. MODULATION OF PHYSIOLOGICAL PATHWAYS

In order to establish a hypothesis whether the cellular homeostasis could be affected by the exposure to TiO_2, we performed a transcriptome analysis. The Metascape bioinformatics analysis revealed that the number of the deregulated genes by TiO_2 in the Caco-2 and HaCaT was small. In the HaCaT cells only 18 genes were differentially expressed after 72h exposure to NM104 particles and in 5 week cultures only 22 genes were significantly differentially deregulated (Table 2A).

Table 2. A: Comparison of deregulated genes in HaCaT after 72h and 28 days of exposure to TiO_2 nanoparticles.

HaCaT 72h				HaCaT 5 weeks			
CTR vs NM104				CTR vs NM104			
	logFC	AveExpr	adj.P.Val		logFC	AveExpr	adj.P.Val
KCNQ1OT1	-3.31	7.82	0.36418	CYR61	-2.37	12.63	0.317204
CKLF	-1.78	9.28	0.046943	LCE2B	-1.99	10.44	0.005788
GP9	-1.77	8.43	0.043415	LCE2A	-1.89	9.71	0.004928
NID2	-1.65	8.28	0.44627	LCE2D	-1.88	8.81	0.001613
IAPP	-1.51	9.04	0.05037	NTS	-1.85	9.51	0.007413
				LCE1B	-1.84	9.49	0.001613
HCG11	1.55	9.92	0.148957	LCE3D	-1.83	13.56	0.002871
IL2RG	1.60	6.82	0.365592	LCE6A	-1.81	10.43	0.004536
HDAC4	1.64	7.84	0.200083	CRCT1	-1.70	12.56	0.002193
RAB40B	2.07	9.68	0.410156	SPRR2G	-1.66	10.67	0.005855
IQCH	2.09	6.99	0.342922	LCE3B	-1.64	10.18	0.000482
C17orf78	2.28	6.58	0.351807	KPRP	-1.61	9.99	0.009753

HaCaT 72h				HaCaT 5 weeks			
CTR vs NM104				CTR vs NM104			
RP11-613C6.2	2.56	6.96	0.375279	LCE3E	-1.59	11.48	0.001613
NTN3	2.59	8.74	0.466499				
SLC28A2	2.75	6.90	0.365877	ADRA2C	1.52	8.17	0.013544
DMRT1	2.93	8.19	0.342556	EGFL6	1.56	6.98	0.005788
IQCF5-AS1	3.26	7.14	0.364675	SOCS2	1.64	9.52	0.000482
TINAG	3.44	7.27	0.300333	FYB	1.75	8.48	0.000795
FGF12	3.88	7.86	0.375765	TAC3	1.79	9.62	0.003955
				ANGPTL 7	1.87	7.48	0.0015
				CYP2F2P	2.07	8.37	0.007362
				DEFB1	2.07	10.33	0.001108
				RNA5-8S5	2.08	13.70	0.013544

Caco-2 cells differentially expressed 26 genes after 72h exposure to E171. After 5 weeks, the number of the differentially expressed genes was reduced to 10 genes incl. genes KEL, PRKA2 and TRPM8 (Table 2B). In particular, biological processes in enterocytes relevant to ion transport and apoptosis were affected.

Table 2. B: Comparison of deregulated genes in Caco-2 (B) cells after 72h and 28 days of exposure to TiO_2 nanoparticles.

Caco-2 72h				Caco-2 5weeks			
ctr vs E171				ctr vs E171			
	logFC	AveExpr	adj.P.Val		logFC	AveExpr	adj.P.Val
SEPT14	-4.14	7.75	0.448409	PRKAA2	-3.41	9.87	0.809995
YWHAE	-3.70	9.08	0.426361	FYN	-3.31	10.28	0.810193
MYSM1	-3.64	9.01	0.467853	KIF11	-3.07	11.13	0.810594
CYP1A1	-3.49	10.67	1.48E-05	DOC2B	-2.81	7.40	0.811225
ZNF772	-3.46	7.25	0.448812				
NAP1L5	-3.15	6.93	0.428142	MFAP3L	1.80	7.72	0.809703
ABHD17C	-3.11	10.72	0.434155	AC141586.5	1.83	7.52	0.811225
LINC00619	-2.95	6.90	0.457121	TRPM8	1.90	6.67	0.809881
CSTF2T	-2.88	10.79	0.463352	CFAP53	2.04	6.80	0.809703
MTF2	-2.42	11.00	0.432766	RP11-137H2.4	2.19	7.05	0.809703
MT2A	-2.15	10.32	0.001471	DGCR9	2.44	6.77	0.809881
HSPA1A	-2.15	13.43	0.001093	KEL	2.48	6.61	0.810251
SIK2	-1.97	8.73	0.481007	TFAP2E	4.28	8.51	0.809703

Caco-2 72h				Caco-2 5weeks
ctr vs E171				ctr vs E171
MT1M	-1.85	7.10	0.024839	
HSPA1B	-1.57	12.54	0.00145	
MT1L	-1.52	8.30	0.001471	
FGFBP1	-1.52	7.96	0.001093	
SESN2	1.62	8.40	0.008815	
SLC7A11	1.64	10.45	0.001566	
HERPUD1	1.66	14.16	0.007115	
BBC3	1.67	10.31	0.016918	
RNA5-8S5	1.68	15.45	0.069814	
CHAC1	1.72	9.30	0.023228	
CEBPB	1.74	13.42	0.005565	
DDIT4	1.79	10.86	0.015598	
SLC38A2	1.84	11.41	0.006595	

A comparison of the deregulated genes from HaCaT and Caco-2 showed very little commonalities of the modification of the gene expression profile (only one gene), suggesting that different biological effects in the two cell lines must be expected (Fig 6).

Figure 6. Comparison of deregulated genes.

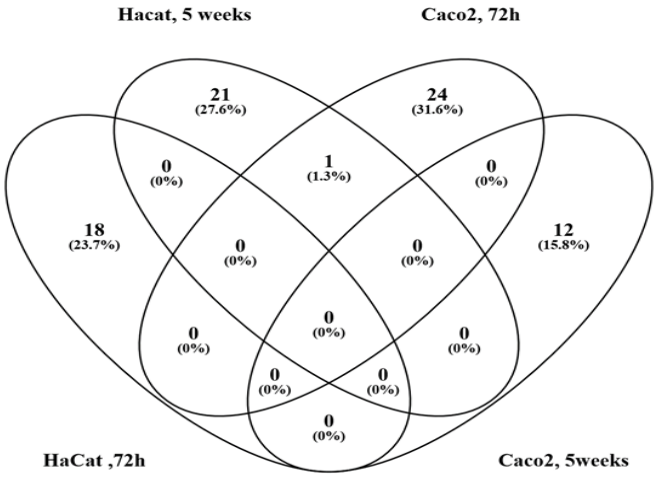

The annotation of the genes to biological pathways elucidated that the modulated genes in long-term cultures of HaCaT cells were involved in keratinogenesis (Fig 7A). Notably, genes deregulated in Caco-2 cells after 72 hours of exposure to the nanoparticles belonged to the biological process (GO:0070059) associated with cellular

stress (Fig.7B). The low level of deregulated genes as well as the lack of common pathways related to e.g. cytotoxicity confirmed our observation in the other in vitro assays.

Fig 7A Biological processes in HaCaT cells modulated after exposure to TiO_2 after 72h and 5 weeks

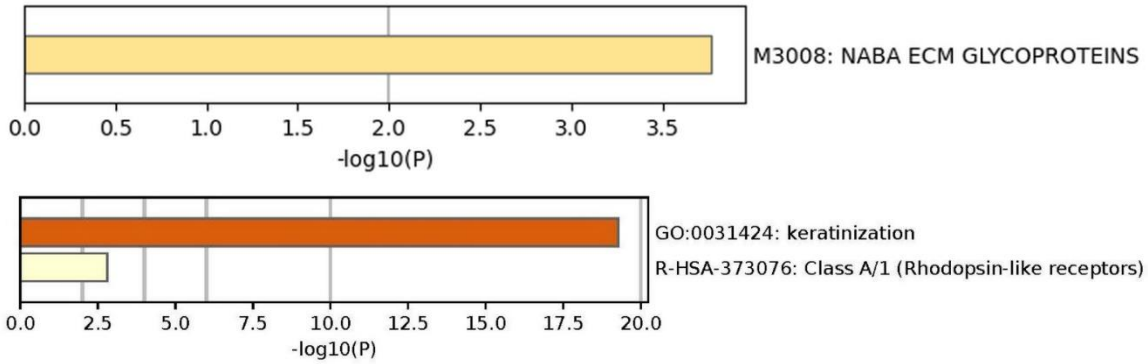

The metascape analysis revealed that the process of keratogenesis (GO: 0031424) was statistically highly enriched with a log10 (P) value of higher than 19.

Fig 7B Biological processes in Caco-2 cells modulated after exposure to TiO_2 after 72h and 5 weeks

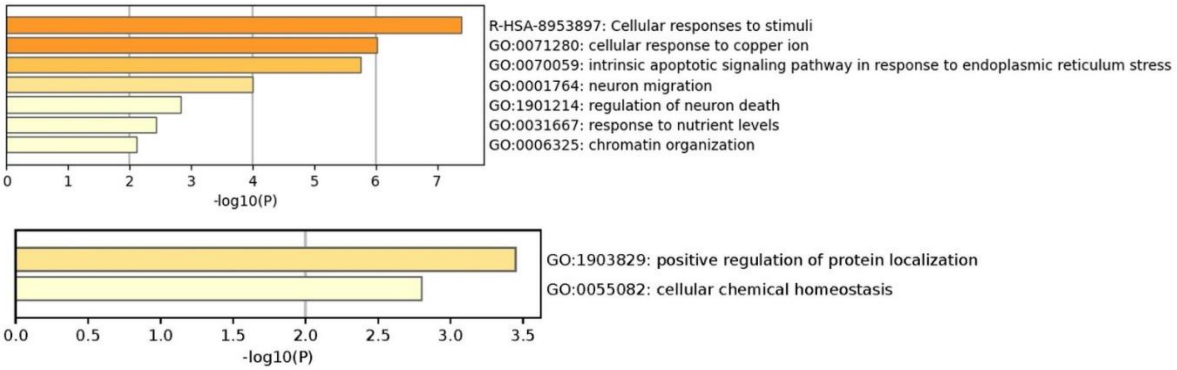

In the metascape analysis demonstrated a modification of pathways involved in cellular responses to stimuli including copper ions in short term cultures. In long-term culture it seems that cells adapted to the stressors and only the cellular chemical homeostasis is changed.

4. Discussion

The accumulation potential of metal oxide nanoparticles such as TiO_2 in human tissues is well-known[19] and currently exploited for various biomedical applications, supporting the development of new diagnostic and therapeutic tools[20]. While the uptake of metal oxide nanoparticles in diseased tissues is desirable for therapeutic applications, the unintentional intracellular accumulation of engineered nanomaterials from medicinal and other consumer products can lead to undesired biological effects in healthy cells[21]. Potential severe adverse effects, either directly or indirectly caused by TiO_2 nanoparticles, such as genotoxicity[22,23], inflammation[24,25] and carcinogenesis[26] could not been ruled out. European regulators suggested applying the precautionary principle leading to classifications and bans of the TiO_2 in consumer products. Since other regions such as the UK or Canada did not

consider sufficient evidence for regulatory actions, TiO_2 in consumer products can still be marketed outside Europe. However, even if there is now an urgent need for a better understanding of potential human hazards of TiO_2 suitable, conclusive and regulatory accepted test methods are lacking so far.

In the present study, we have investigated the capability of different cell models to internalize and store different forms of TiO_2 for a culture period of up to 5 weeks. Acccording to our knowledge, there are no other studies that quantifed the accumulated TiO_2 nanoparticles in long-term cell cultures by using radiotracer. Such *in vitro* platforms are a prerequisite to elucidate mechanisms of potential single and repeated dose effects of nanomaterials such as TiO_2 nanoparticles in long-term cell cultures[21] but are also offering opportunities for efficacy testing of TiO_2 as nanocarrier for drug delivery systems.

As previously reported, we could confirm that TiO_2 at a concentration of 100 µg/mL, did not exhibit any significant cellular effects related to the viability[27], morphology, cell transformation and transepithelial electric resistance of the cellular barrier but we were able to quantify TiO_2 in long-term cell cultures by using radiolabelled material. In order to establish a hypothesis driven approach supporting a better understanding of the intracellular stress response of TiO_2 accumulation in cell cultures, we analysed modifications of the transcriptome in monocultures repeatedly treated with TiO_2 and kept in culture for 5 weeks[14]. The transcriptomics study revealed only slight deregulation of genes, but interestingly, the gene expression profiles differed in short-term (72h) and long-term (5 weeks) cell-cultures. The gene expression profiles also differed between cell types suggesting that the effects of nanoparticles depend on the accumulation of material and the physiological role of the cell in the tissue.

The accumulation of NM 104 in keratinocytes for example led to a significant modulation of the genes relevant for the process of keratinogenesis. Keratinocytes are involved in the formation of the four layers of the epidermis. During the keratinization process, undifferentiated keratinocytes located in the epidermis proliferate and migrate to the stratum granulosum layer. During the migration process, the cells differentiate and reach the superficial layer, before they are embedded in a dense lipid transcellular matrix[28,29]. Increased keratinization was also observed in lung cells treated with TiO_2[19].

The transcriptomic profiles of Caco-2 vary depending on the duration of the cell culture after exposure to TiO_2. The transcriptome of Caco-2 cells 72h after exposure for example suggested the induction of epigenetic changes as GO: 0006325 (chromatin organization) is enriched (see Fig 6B). Genes like the Metal Response Element Binding Transcription Factor 2 (MTF2) that is necessary for the polycomb repressive complex 2 (PRC2)-mediated epigenetic chromatin modification via histone H3-K27methylation were identified[30]. Other genes such as Myb Like, SWIRM and MPN Domains 1 (MYSM1) that promotes deubiquitination of the monoubiquitinated histone H2A are leading to a separation of histone H1 from the nucleosome[31]. An abnormal DNA CpG sites methylation status represents one key epigenetic mechanism. Recently it was shown

that the Nucleosome Assembly Protein 1 like 5 (NAP1L5), an imprinted gene, was hypomethylated under pathological conditions, suggesting the involvement of this e gene in epigenetic-induced chromosomal alterations. Already Stoccoro et al.,[32] and Pogribna et al.,[33,34] reported about epigenetic modifications in mammalian cells after exposure to TiO_2 particles.

In addition, the transcriptome analysis showed a statistically significant enrichment of GO term 0070059 pointing to an increased intrinsic apoptosis in Caco-2 monocultures due to ER stress. Already Hu et al.[35] reported ER stress after treatment of rats with TiO_2 for 26 weeks. ER stress is normally induced by the reactive oxygen species (ROS)[36] and characterized by the accumulation of unfolded/misfolded proteins in ER, oxidative stress, nutrient deprivation and disturbances in the energy metabolism, as well as by calcium depletion and by DNA damage[37]. Our analysis revealed a deregulation of a number of genes involved in apoptosis and ER stress such as the BCL2 Binding Component 3 (BBC3) that belongs to the BCL-2 family and encodes for a pro-apoptotic protein. As part of the BCL-2 family, the cellular activation of BBC3 via stress molecules causes endoplasmic reticulum stress (ERS), thereby resulting in apoptosis[38]. Similarly, the activation of the ChaC Glutathione Specific Gamma-Glutamylcyclotransferase 1 (CHAC1) signalling pathway via ROS can result in the activation of the ERS and cellular apoptosis[39]. Other observed modifications e.g. the DDIT4 expression is referring to several cellular stress mechanisms resulting in ERS[40] and finally, the Homocysteine Inducible ER Protein With Ubiquitin Like Domain 1 (HERPUD1) is acting as an antiapoptotic protein against ROS-induced ER stress[41]. Some of the described mechanisms were also observed in A549 lung cancer cells and endothelial cells, after exposure to silica nanoparticles. The expression of genes participating in the response to nutrient levels (GO:0031667) is supporting the evidence of ROS productions since the link between nutrient responses and ROS production is well known[42]. The induction of apoptosis can lead to a disturbance of the equilibrium between cell death and cell renewal of the intestinal epithelium. Dysregulated apoptotic processes have been reported in a number of pathological bowel diseases[43] including coeliac disease, and ulcerative colitis (UC).

Moreover, the analysis of the transcriptome data indicated modifications of genes involved in cellular responses of Caco-2 cells to copper ions. Copper is an essential trace element, which is cytotoxic at higher concentrations. Dysregulations causes severe consequences by hepatic and neurological disorders such as the Wilson disease[44]. Usually, specific transport proteins such as the CTR1 are involved, and the influx and efflux of trace elements is strongly controlled in order to keep the homeostasis in the cell. However, the capability of TiO_2 nanoparticles to absorb copper ions opens up another route of internalisation for copper ions e.g through enterocytotic pathways[45]. The increase uptake of copper ions through the so-called Trojan horse effect would explain the upregulation of genes involved in cellular responses to copper ions.

Nevertheless, as for keratinocytes, the most remarkable observation was storage of TiO_2 particles in CaCo-2 cells cultured for 5 weeks. The accumulated TiO_2 nanoparticles in the

cells suggested an impairment of lysosomal degradation pathways that are known to play a vital role in cellular homeostasis. In the present study, a number of genes related to cellular homeostasis were dysregulated (Fig 6B). Lysosomal dysfunction after repeated dosing of cells were already reported by Stern et al. 2012 and by Popp et al. 2018[46,47]. Any impairment or inefficiencies in this degradation system can be associated with the development of a variety of human diseases, ranging from neurodegenerative disorders to cancer.

5. Conclusion

TiO_2 is a challenging nanomaterial whose use is the subject of much controversy since existing research has not yet reached firm conclusions regarding the potential risks. Our study supported a number of mechanistic observations that can potentially lead to an adversity and were already highlighted by EFSAs panel on food additives and Flavourings (FAF)[1]. Transcriptome analyses of the various cell types suggested that the accumulation of the material might lead various impairments in cellular homeostasis. However, future research is needed to investigate to what extend dysregulated processes initiated by the accumulated material must be seen as the origin of lesions and other adversities observed in vivo.

Conflict of Interest:

The authors have no conflicts of interest to declare. The views and opinions expressed in this article are those of the authors and do not necessarily reflect the official position of their organisations. Illustrations in Figure 1 obtained publication licences (XT265QAGQB, FP265QAV06, WO265QB5M7) from biorender.

Funding:

None

Acknowledgements

The authors would like to thank Pierre Lau Poui Cheung for his biostatistical analysis.

References:

1. Safety assessment of Titanium dioxide (E171) as a food additive. Scientific Opinion on the safety of titanium dioxide (E171). :4502. https://doi.org/10.2903/j.efsa.2021.6585

2. Baranowska-Wójcik E, Szwajgier D, Oleszczuk P, Winiarska-Mieczan A. Effects of Titanium Dioxide Nanoparticles Exposure on Human Health-a Review. *Biol Trace Elem Res*. 2020;193(1):118-129. doi:10.1007/s12011-019-01706-6

3. Commission Delegated Regulation (EU) 2020/217 of 4 October 2019. Published 2020. https://www.legislation.gov.uk/eur/2020/217/contents

4. Final feedback from European Medicine Agency (EMA) to the EU Commission request to evaluate the impact of the removal of titanium dioxide from the list of authorised food additives on medicinal products. *EMA*. 2021;(504010).

5. SCIENTIFIC COMMITTEE ON CONSUMER SAFETY (SCCS) Request for a scientific opinion on the safety of Titanium dioxide (TiO2) (CAS/EC numbers 13463-67-7/236-675-5, 1317-70-0/215-280- 1, 1317-80-2/215-282-2) in cosmetic products.

6. *European Commission (2020a) Chemicals – Strategy for Sustainability (Toxic-Free EU Environment).*2021. https://ec.europa.eu/info/law/better-regulation/have-your-say/initiatives/12264-Chemicals-strategy-forsustainability-toxic-free-EU-environment- en

7. Food Directorate HC. State of the science of titanium dioxide (TiO_2) as a food additive. Published online 2022. https://publications.gc.ca/site/eng/9.912399/publication.html

8. Kreyling WG, Holzwarth U, Haberl N, et al. Quantitative biokinetics of titanium dioxide nanoparticles after intravenous injection in rats: Part 1. *Nanotoxicology*. 2017;11(4):434-442. doi:10.1080/17435390.2017.1306892

9. Geraets L, Oomen AG, Krystek P, et al. Tissue distribution and elimination after oral and intravenous administration of different titanium dioxide nanoparticles in rats. *Part Fibre Toxicol*. 2014;11(1):30. doi:10.1186/1743-8977-11-30

10. Disdier C, Devoy J, Cosnefroy A, et al. Tissue biodistribution of intravenously administrated titanium dioxide nanoparticles revealed blood-brain barrier clearance and brain inflammation in rat. *Part Fibre Toxicol*. 2015;12(1):27. doi:10.1186/s12989-015-0102-8

11. Coméra C, Cartier C, Gaultier E, et al. Jejunal villus absorption and paracellular tight junction permeability are major routes for early intestinal uptake of food-grade TiO2 particles: an in vivo and ex vivo study in mice. *Part Fibre Toxicol*. 2020;17(1):26. doi:10.1186/s12989-020-00357-z

12. Riedle S, Wills JW, Miniter M, et al. A Murine Oral-Exposure Model for Nano- and Micro-Particulates: Demonstrating Human Relevance with Food-Grade Titanium Dioxide. *Small*. 2020;16(21):2000486. doi: https://doi.org/10.1002/smll.202000486

13. Winkler HC, Notter T, Meyer U, Naegeli H. Critical review of the safety assessment of titanium dioxide additives in food. *J Nanobiotechnology*. 2018;16(1):51. doi:10.1186/s12951-018-0376-8

14. Berggren E, White A, Ouedraogo G, et al. Ab initio chemical safety assessment: A workflow based on exposure considerations

and non-animal methods. *Comput Toxicol (Amsterdam, Netherlands)*. 2017;4:31-44. doi: 10.1016/j.comtox.2017.10.001

15. Geiss O, Ponti J, Senaldi C, et al. Characterisation of food grade titania with respect to nanoparticle content in pristine additives and in their related food products. *Food Addit Contam Part A*. 2020;37(2):239-253. doi:10.1080/19440049.2019.1695067

16. OECD. *Study Report and Preliminary Guidance on the Adaptation of the In Vitro Micronucleus Assay (OECD TG 487) for Testing of Manufactured. Series on Testing and Assessment No. 359 Nanomaterials.*; 2022. https://one.oecd.org/document/env/cbc/mono(2022)15/en/pdf

17. Forcella M, Lau P, Oldani M, et al. Neuronal specific and non-specific responses to cadmium possibly involved in neurodegeneration: A toxicogenomics study in a human neuronal cell model. *Neurotoxicology*. 2020;76:162-173. doi:10.1016/j.neuro.2019.11.002

18. Zhou Y, Zhou B, Pache L, et al. Metascape provides a biologist-oriented resource for the analysis of systems-level datasets. *Nat Commun*. 2019;10(1):1523. doi:10.1038/s41467-019-09234-6

19. *IARC Monographs on the Evaluation of Carcinogenic Risks to Humans.*; 2006.

20. Akram MW, Raziq F, Fakhar-e-Alam M, et al. Tailoring of Au-TiO2 nanoparticles conjugated with doxorubicin for their synergistic response and photodynamic therapy applications. *J Photochem Photobiol A Chem*. Published online 2019.

21. Gunduz N, Ceylan H, Guler MO, Tekinay AB. Intracellular Accumulation of Gold Nanoparticles Leads to Inhibition of Macropinocytosis to Reduce the Endoplasmic Reticulum Stress. *Sci Rep*. 2017;7(1):40493. doi:10.1038/srep40493

22. Khlebtsov N, Dykman L. Biodistribution and toxicity of engineered gold nanoparticles: a review of in vitro and in vivo studies. *Chem Soc Rev*. 2011;40(3):1647-1671. doi:10.1039/c0cs00018c

23. Kirkland D, Aardema MJ, Battersby R V, et al. A weight of evidence review of the genotoxicity of titanium dioxide (TiO2). *Regul Toxicol Pharmacol*. 2022;136:105263. doi: https://doi.org/10.1016/j.yrtph.2022.105263

24. Cao X, Han Y, Gu M, et al. Foodborne Titanium Dioxide Nanoparticles Induce Stronger Adverse Effects in Obese Mice than Non-Obese Mice: Gut Microbiota Dysbiosis, Colonic Inflammation, and Proteome Alterations. *Small*. 2020;16(36):e2001858. Doi :10.1002/smll.202001858

25. Nogueira CM, de Azevedo WM, Dagli MLZ, et al. Titanium dioxide induced inflammation in the small intestine. *World J Gastroenterol*. 2012;18(34):4729-4735. doi:10.3748/wjg.v18.i34.4729

26. Bettini S, Boutet-Robinet E, Cartier C, et al. Food-grade TiO(2) impairs intestinal and systemic immune homeostasis, initiates preneoplastic lesions and promotes aberrant crypt development in the rat colon. *Sci Rep*. 2017;7:40373. doi:10.1038/srep40373

27. Crosera M, Prodi A, Mauro M, et al. Titanium Dioxide Nanoparticle Penetration into the Skin and Effects on HaCaT Cells. *Int J Environ Res Public Health*. 2015;12(8):9282-9297. doi:10.3390/ijerph120809282

28. Baroni A, Buommino E, Gregorio V De, Ruocco E, Ruocco V, Wolf R. Structure and function of the epidermis related to barrier

properties. *Clin Dermatol*. 2012;30 3:257-262.

29. Tricarico PM, Mentino D, De Marco A, et al. Aquaporins Are One of the Critical Factors in the Disruption of the Skin Barrier in Inflammatory Skin Diseases. *Int J Mol Sci*. 2022;23(7). doi:10.3390/ijms23074020

30. Khan A. Aziz, Ham S., Yen L., Lee H. Lim, Huh J., Jeon H., Kim M. Hee RT. A novel role of metal response element binding transcription factor 2 at the Hox gene cluster in the regulation of H3K27me3 by polycomb repressive complex 2. *Oncotarget*. 2018;9:26 572-26585.

31. Zhu P, Zhou W, Wang J, et al. A histone H2A deubiquitinase complex coordinating histone acetylation and H1 dissociation in transcriptional regulation. *Mol Cell*. 2007;27(4):609-621. doi:10.1016/j.molcel.2007.07.024

32. Stoccoro A, Di Bucchianico S, Coppedè F, et al. Multiple endpoints to evaluate pristine and remediated titanium dioxide nanoparticles genotoxicity in lung epithelial A549 cells. *Toxicol Lett*. 2017;276:48-61. doi:10.1016/j.toxlet.2017.05.016

33. Pogribna M, Koonce NA, Mathew A, et al. Effect of titanium dioxide nanoparticles on DNA methylation in multiple human cell lines. *Nanotoxicology*. 2020;14(4):534-553. doi:10. 1080/17435390.2020.1723730

34. Pogribna M, Hammons G. Epigenetic Effects of Nanomaterials and Nanoparticles. *J Nanobiotechnology*. 2021;19(1):2. doi:10.118 6/s12951-020-00740-0

35. Hu H, Li L, Guo Q, et al. RNA sequencing analysis shows that titanium dioxide nanoparticles induce endoplasmic reticulum stress, which has a central role in mediating plasma glucose in mice. *Nanotoxicology*. 2018;12(4):341-356. doi:10.1080/17435390.2018.1446560

36. Ong G, Logue SE. Unfolding the Interactions between Endoplasmic Reticulum Stress and Oxidative Stress. *Antioxidants (Basel, Switzerland)*. 2023;12(5). doi:10.3390/ antiox12050981

37. Liu M qing, Chen Z, Chen L xi. Endoplasmic reticulum stress: a novel mechanism and therapeutic target for cardiovascular diseases. *Acta Pharmacol Sin*. 2016;37(4):425-443. doi:10.1038/aps.2015.145

38. Pihán P, Carreras-Sureda A, Hetz C. BCL-2 family: integrating stress responses at the ER to control cell demise. *Cell Death Differ*. 2017;24(9):1478-1487. doi:10.1038/cdd.2017.82

39. Cui Y, Zhou X, Chen L, et al. Crosstalk between Endoplasmic Reticulum Stress and Oxidative Stress in Heat Exposure-Induced Apoptosis Is Dependent on the ATF4–CHOP–CHAC1 Signal Pathway in IPEC-J2 Cells. *J Agric Food Chem*. 2021;69(51):15495-15511. doi:10.1021/acs.jafc.1c03361

40. Fattahi F, Saeednejad Zanjani L, Habibi Shams Z, et al. High expression of DNA damage-inducible transcript 4 (DDIT4) is associated with advanced pathological features in the patients with colorectal cancer. *Sci Rep*. 2021;11(1):13626. doi:10.1038/s415 98-021-92720-z

41. Paredes F, Parra V, Torrealba N, et al. HERPUD1 protects against oxidative stress-induced apoptosis through downregulation of the inositol 1,4,5-trisphosphate receptor. *Free Radic Biol Med*. 2016;90:206-218. doi:https://doi.org/10.1016/j.freeradbiomed. 2015.11.024

42. Luo H, Chiang HH, Louw M, Susanto A,

Chen D. Nutrient Sensing and the Oxidative Stress Response. *Trends Endocrinol Metab*. 2017;28(6):449-460. doi:10.1016/j.tem.2017.02.008

43. Ramachandran A, Madesh M, Balasubramanian KA. Apoptosis in the intestinal epithelium: its relevance in normal and pathophysiological conditions. *J Gastroenterol Hepatol*. 2000;15(2):109-120. doi:10.1046/j.1440-1746.2000.02059.x

44. Nishito Y, Kambe T. Absorption Mechanisms of Iron, Copper, and Zinc: An Overview. *J Nutr Sci Vitaminol (Tokyo)*. 2018;64(1):1-7. doi:10.3177/jnsv.64.1

45. Fan W, Cui M, Liu H, et al. Nano-TiO2 enhances the toxicity of copper in natural water to Daphnia magna. *Environ Pollut*. 2011;159(3):729-734. doi:10.1016/j.envpol.2010.11.030

46. Stern ST, Adiseshaiah PP, Crist RM. Autophagy and lysosomal dysfunction as emerging mechanisms of nanomaterial toxicity. *Part Fibre Toxicol*. 2012;9(1):20. doi: 10.1186/1743-8977-9-20

47. Popp L, Tran V, Patel R, Segatori L. Autophagic response to cellular exposure to titanium dioxide nanoparticles. *Acta Biomater*. 2018;79:354-363. doi:https://doi.org/10.1016/j.actbio.2018.08.021

Supplementary material

Radioactive Labelling and Characterisation of TiO2 nanoparticles

RADIOLABELING OF TiO2-NPS VIA PROTON IRRADIATION

The proton irradiation of the TiO_2 nanoparticles was performed on batches of 27 mg of material creating $^{[48V]}V$ atoms by the nuclear reaction $^{[48V]}Ti(p,n)^{[48V]}V$ following the previously described method[1–3]. The irradiations resulted in an activity concentration of 6.56 MBq/mg for the NM104 NPs at the end of bombardment and of 6.27 MBq/mg for the NM105 at the end of bombardment.

TiO2 NP CHARACTERISATION AFTER PROTON BOMBARDMENT

The physicochemical characterisation of cold and $^{[48V]}V$-radiolabelled types of the TiO_2 nanoparticles did not show meaningful differences by using different methodologies, such as dynamic light scattering (DLS), X-ray diffraction (XRD) and transmission electron microscopy (TEM). Especially we have not found any indications for thermal alterations due to dissipated proton beam energy during proton irradiation. Such alterations could be detected by emerging additional diffraction peaks or by a decreasing width of the X-ray diffraction peaks as extensively studied for NM105[1]. Moreover, for the material NM105, which contains two phases of titania (anatase and rutile), the ratios of the diffracted X-ray intensity from both phases did not change.

DLS MEASUREMENTS

The DLS measurements were performed with Zetasizer Nano ZS system (Malvern Instruments: Malvern, UK) in the stock suspension after being diluted at 10 µg/µL in deionized water. For the DLS measurements the NM104 and NM105 nanoparticles were sonicated for 40 minutes at 40% of amplitude using a Digital Sonifier 450 / 400 W from Branson (corresponding to 2.3 W acoustic power in a total volume of 20 mL). The dispersion was vortex mixed for 1 min and directly used for DLS and ζ-potential measurements (and the preparation of XRD specimens). The results are presented in Figure 1 and Table 1.

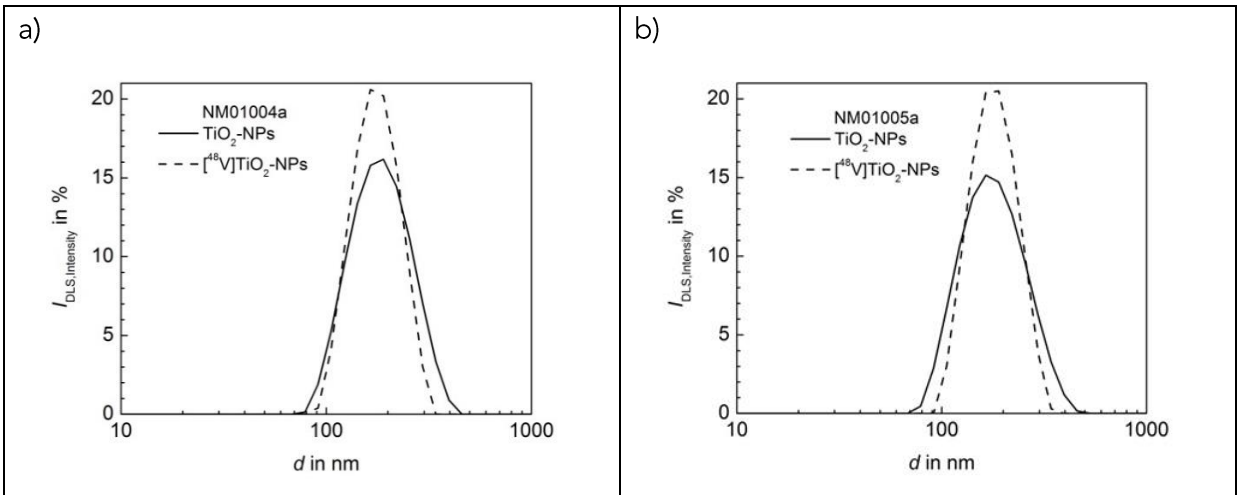

Figure 1: Hydrodynamic particle size given as size – intensity distribution for the materials (a) NM104 and (b) NM105 before and after labelling with $^{[48V]}V$ by proton irradiation.

Table 1: Tabulated DLS results for type NM104 and NM105 TiO_2 nanoparticles before and after $^{[48V]}V$ labeling by proton irradiation. The slight increase of the z-average values after proton irradiation can be explained by the presence of a tiny fraction of large agglomerates that are responsible for a second peak around 1000 nm that contributes less than 0.2% to the intensity

Material	z-average	main peak	PDI	ζ-potential
NM104	(155.1±4.4)nm	(158.8±16.2)nm	0.234±0.034	(36.9±0.3)mV
$^{[48V]}$NM104	(214.7±10.8)nm	(176.1±1.9)nm	0.320±0.040	(35.0±1.1)mV
NM105	(169.4±3.4)nm	(203.6±8.6)nm	0.174±0.031	(23.1±0.7)mV
$^{[48V]}$NM105	(194.6±11.7)nm	(185.0±6.5)nm	0.241±0.019	(31.7±0.5)mV

The ζ-potential measurements of the non-labelled materials correspond to the values reported earlier[4]. The slightly decreased ζ-potential of $^{[48V]}TiO_2$ type NM104 has most likely no consequences for the nanoparticle stability while the increase of the ζ-potential of radiolabelled NM105 by about 8 mV should improve the stability of the nanoparticle suspension[4].

XRD MEASUREMENTS

X-ray diffraction scans were performed operating in the grazing-angle X-ray diffraction mode (GAXRD) employing Cu-Kα radiation k = 1.5418 Å at a tube voltage of 35 keV and current of 30 mA. The diffractometer has an instrumental resolution of about 0.2° and is equipped with a solid state detector for resolving the Kα-radiation and for improved signal/noise ratio. In order to have flat nanocrystalline surfaces for the XRD examinations the recovered nanoparticles have been deposited onto a Si-wafer[1]. For this purpose nanoparticles were suspended in water and a droplet of the suspension was deposited on a Si-wafer. After evaporation of the water the nanoparticles have been fixed by a drop of PMMA (Poly(methyl methacrylate)) dissolved in anisol.

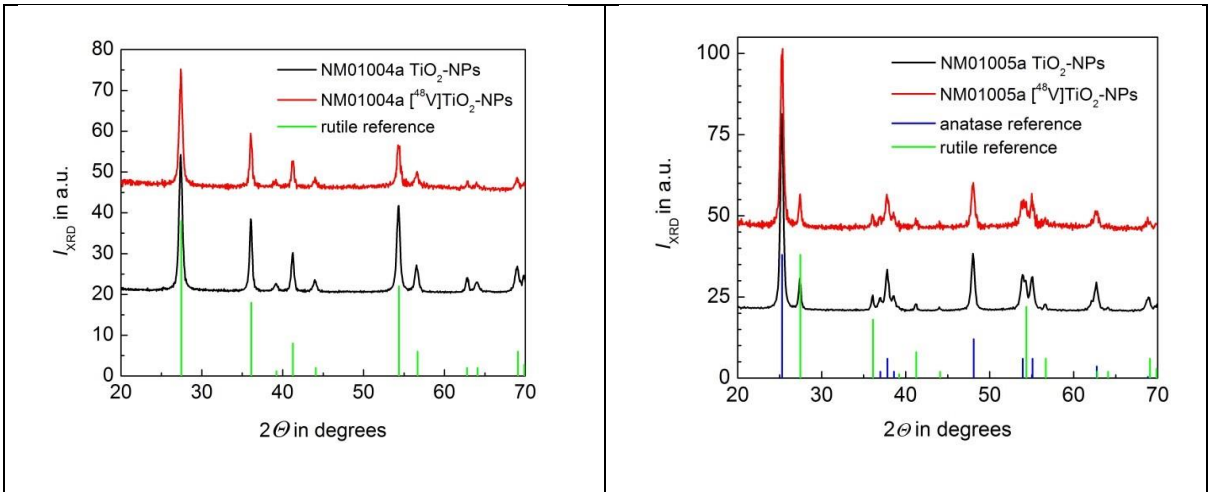

Figure 2: X-ray diffraction patterns of as-received and $^{[48V]}V$-radiolabelled type NM105 TiO_2 nanoparticles. The references for the rutile diffraction maxima are indicated.

Figure 3: X-ray diffraction patterns of as-received and $^{[48V]}V$ radiolabelled type NM105 TiO_2 nanoparticles. The references for the anatase and rutile diffraction maxima are indicated.

The results presented in Figures 2 and 3 show no differences between the unlabeled and the $^{[48V]}$V-radiolabelled types of the TiO_2 nanoparticles. Especially there are now indications of thermal alterations due to dissipated proton beam energy during proton irradiation. The increased noise visible in the figures for the radiolabelled nanoparticles is due to the very small amount of material that was sacrificed for the XRD-study.

The XRD patterns correspond qualitatively and quantitatively to those presented by Rasmussen et al.,[4].

TRANSMISSION ELECTRON MICROSCOPY

Figures 4 and 5 indicate that the radiolabelling of the TiO_2 nanoparticles does not change the appearance of the nanoparticles. The TEM micrographs are qualitatively identical with those presented by Rasmussen et al.[4] in the titania characterisation report. A quantitative analysis of NM104 $^{[48V]}$TiO2 and NM105 $^{[48V]}TiO_2$ nanoparticles as shown in Figs 6 and 7 yielded values of (27.3±7.4)nm and (22.5±6.5)nm , respectively. This agrees well with the data reported by Rasmussen et al.[4] where the TEM analysis of NM104 and NM105 is summarized as (27±10) nm and (21±9) nm, respectively. Thus, also the TEM analysis gives no indication for qualitative or quantitative changes of the nanoparticles introduced by the proton irradiation.

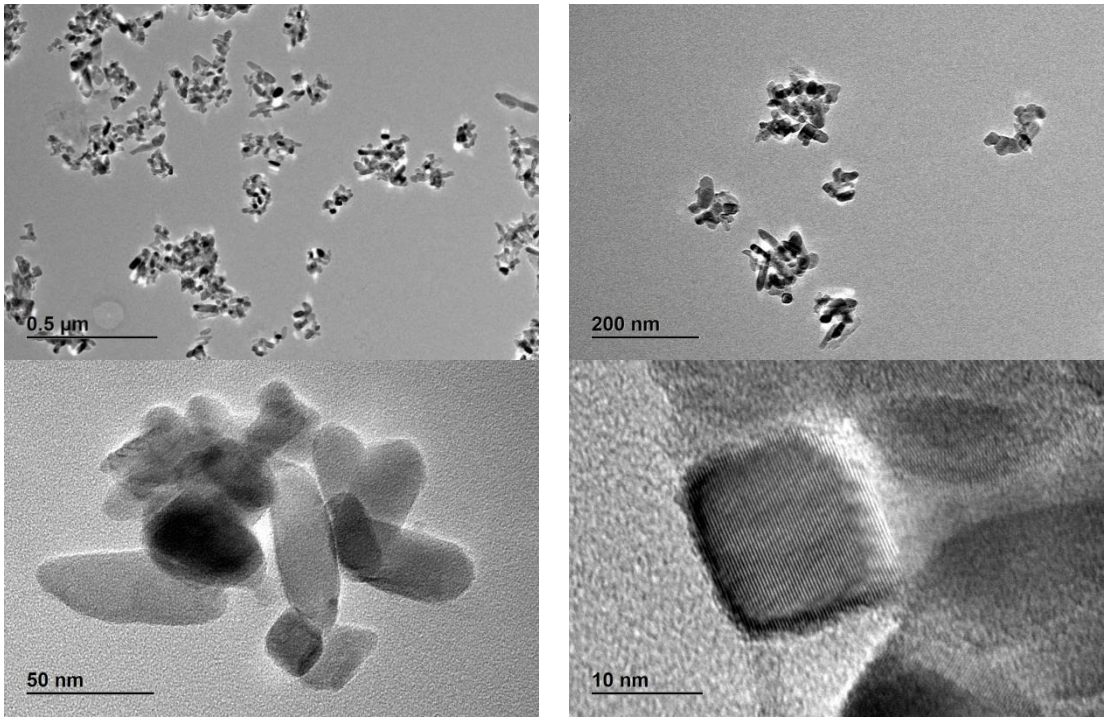

Figure 4: TEM study of $^{[48V]}$V radiolabelled NM104 TiO_2 nanoparticles

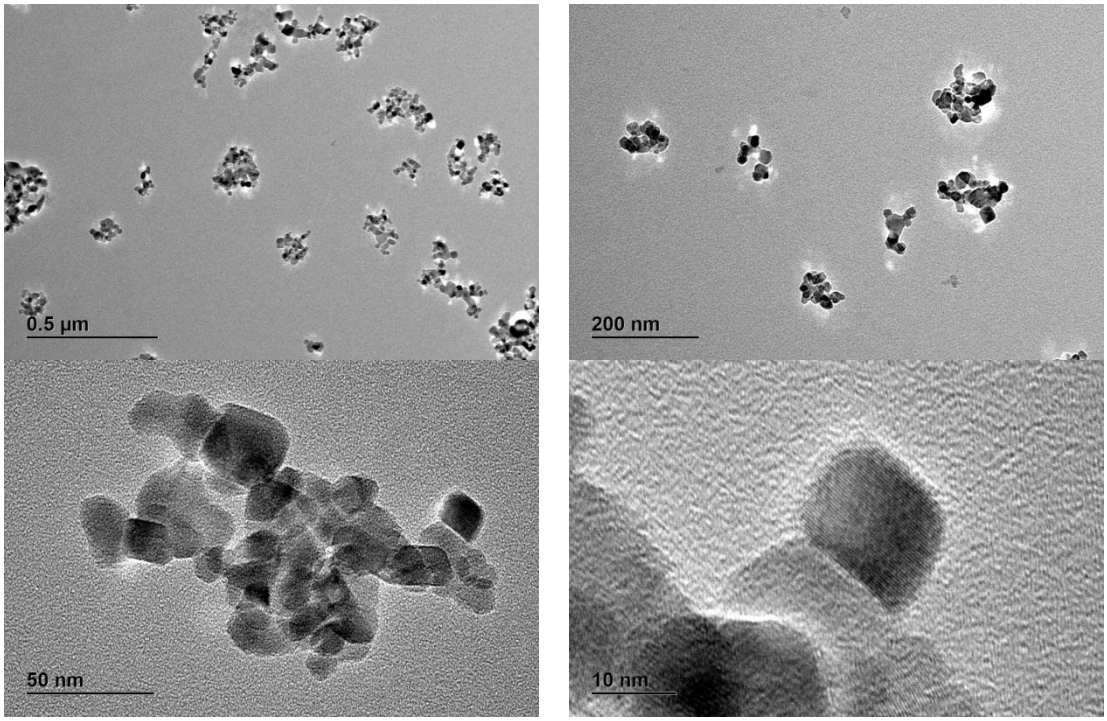

Figure 5: TEM study of $^{[48V]}V$ radiolabelled NM105 TiO_2 nanoparticles

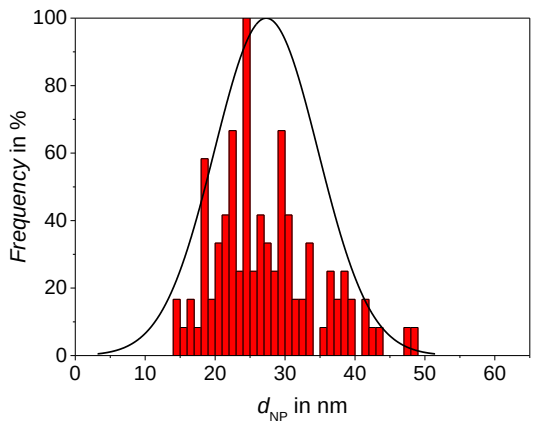

Figure 6: Size distribution determined from the evaluation of 100 proton irradiated NM104 nanoparticles by TEM. The average size of the nanoparticles was determined as (27.3±7.4) nm. The evaluated nanoparticles ranged from 18.8 nm to 48.4 nm. The frequency is normalized to the nanoparticles with the most frequent dNP.

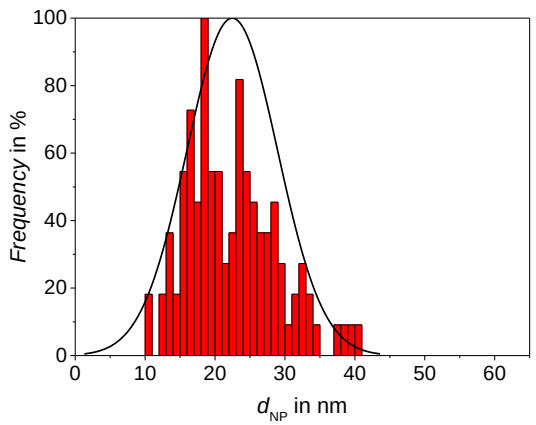

Figure 7: Size distribution determined from the evaluation of 100 proton irradiated NM105 nanoparticles by TEM. The average size of the nanoparticles was determined as (22.5±6.5) nm. The evaluated nanoparticles ranged from 10.6 nm to 40.4 nm. The frequency is normalized to the nanoparticles with the most frequent dNP.

COLONY FORMING EFFICIENCY (CFE) TEST

The protocol of the Colony Forming Efficiency (CFE) assay was previously described[5–7]. In brief, HaCat, Caco-2 and Balb/3T3 cells were seeded at a density of 200 cells/dish (60x15 mm Petri dish, 19.3 cm^2 bottom surface area, Falcon, Italy). Cell cultures were treated with 100µg/mL TiO_2NPs following the exposure protocols 1 and 2 as described in Fig.1. After 8 days the colonies were fixed with paraformaldeyde (4%), stained with Giemsa (10%) and automatically counted

with Gelcount. Na_2CrO_4 (10^{-3}M) was used as cytotoxic positive control (CAS N.10034-82-9, Cat N. 013453, AlfaAesar, Johnson Matthey GmbH).

TiO_2 did not induce observable toxicity at the highest concentration of 100µg/ml TiO_2. This observation was confirmed in a systematic assessment by using the established colony forming assay. Balb/3T3 cells, CaCo-2 cells and HaCat were exposed for 72h to NM104 and NM105 $Ti0_2$ in a concentration range starting from 10 to 100µg/ml. Furthermore, the lack of inducing cytotoxicity of both materials was proven by measuring the number of PI stained cells by using flow cytometry analysis. (data not shown)

CELL TRANSFORMATION ASSAY (CTA)

The morphological neoplastic transformation potentially induced by TiO_2 NPs in combination with UV exposure, was evaluated by Cell Transformation Assay (CTA).

Experiments were performed as described in Tanaka et al.[8] and Ponti et al.,[9] . In summary, 2×10^4 Balb/3T3 cells were seeded in 6 mL of complete fresh medium Minimum Essential Medium (MEM) 1×supplemented with 10% (v/v), fetal bovine serum-NZ origin and antibiotics (10,000 U/mL penicillin and 10,000 g/mL streptomycin) in 100 mm-Petri dish (5 replicates per concentration). After 24 h (day 1 – D1), medium was replaced and fresh medium containing TiO_2 NP suspensions at a concentration of 100 µg/mL was administered Non-treated Balb/3T3 cells and cells exposed to 2 µg/mL methylcholanthrene (Sigma–Aldrich; Saint Louis, MO, USA), which is a well-known carcinogenic compound, were used as negative and positive controls, respectively. After the exposure to TiO2 the cells were exposed for 5 min to UV light. Neither NM104 nor NM105 induced the formation of type-III foci in Balb/3T3 cells in vitro under the selected experimental settings.

IMMUNOHISTOCHEMISTRY

Balb/3T3 cells were seeded at a density of 1.5 x 10^5 cells/well in 400uL of complete medium on 4-chamber polystyrene vessel tissue culture-treated glass slides (BD Falcon, Italy). 24h after seeding, cells were treated as described above in the treatment protocol for the CTA assay.

After 5 weeks in culture, cells were washed 3 times in PBS to remove residual dye and unbound particles, fixed with 4% (v/v) paraformaldehyde in PBS and permeabilised with 0.1% (v/v) Triton X-100 in PBS (Sigma-Aldrich, Italy). To delimit cell boundaries and highlight the cytoskeleton shape, the actin filaments were stained for 40 min at room temperature with TRITC-conjugated Phalloidin (CHEMICON International) diluted 1:500 in PBS. The nuclei were counterstained with DAPI dye (Sigma, Italy), diluted 1:2000 in PBS. After staining, the cells were washed in PBS and mounted for microscopy. Images were acquired with an Axiovert 200 M inverted microscope equipped with ApoTome slide module and Axiovision 4.8 software (Carl Zeiss; Jena, Germany), using a 40×/1.0 objective lens.

No morphological changes could be detected in Balb/3T3 cells after treatment with NM104 nanoparticles.

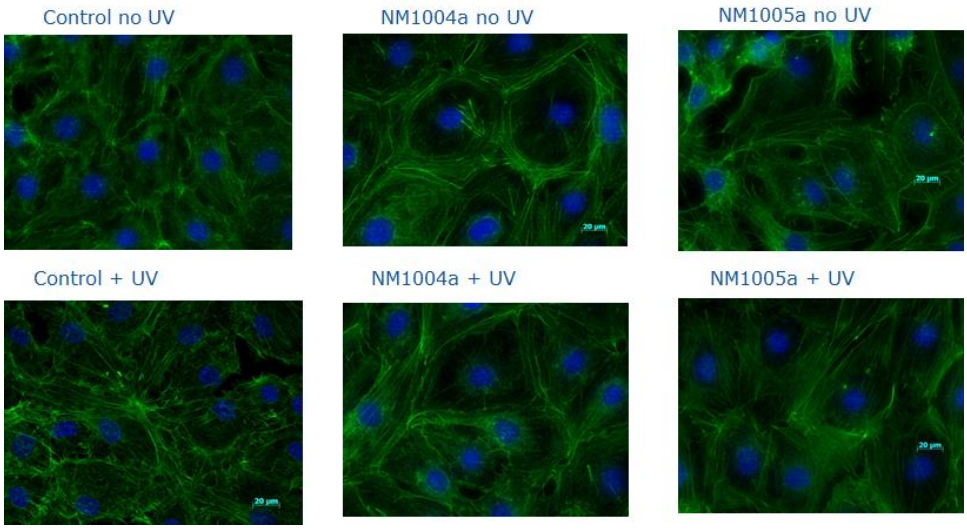

Balb/3T3 cells were seeded at a density of 1.5 x 10^5 cells/well on 4-chamber polystyrene vessel tissue culture-treated glass slides (BD Falcon, Italy) and treated as described in protocol 2 (Fig 2B) 2. After 5 weeks in culture, cells were washed 3 times in PBS to remove residual dye and unbound particles, fixed with 4% (v/v) paraformaldehyde in PBS and permeabilised with 0.1% (v/v) Triton X-100 in PBS (Sigma-Aldrich, Italy). To delimit cell boundaries and highlight the cytoskeleton shape, the actin filaments were stained for 40 min at room temperature with TRITC-conjugated Phalloidin (CHEMICON International) diluted 1:500 in PBS. The nuclei were counterstained with DAPI dye (Sigma, Italy), diluted 1:2000 in PBS. After staining, the cells were washed in PBS and mounted for microscopy. Images were acquired with an Axiovert 200 M inverted microscope equipped with ApoTome slide module and Axiovision 4.8 software (Carl Zeiss; Jena, Germany), using a 40×/1.0 objective lens.

FLOW CYTOMETRY

After the exposure to TiO_2 NPs in 10 cm dishes see exposure protocols 1-3, cell viability was measured trough flow cytometry using PI solution. Cells were washed with PBS, detached with trypsin, counted with Newbauer chamber manually, centrifuged and washed again in PBS. 10^6 cells were resuspended in PBS containing PI (dilution 1:1000) and incubated for 1 minute in the dark.

Cells were transferred into flow cytometry tubes for analysis. Flow cytometry was performed using a CyFlow™ Space Flow Cytometer (https://us.sysmex-flowcytometry.com/instruments/cyflow-space/1390/cyflow-space), measuring 10,000 events per tube. Three biological replicates were performed.

References

1. Holzwarth U, Bulgheroni A, Gibson N, et al. Radiolabelling of nanoparticles by proton irradiation: temperature control in nanoparticulate powder targets. *J Nanoparticle Res.* 2012;14(6):880. doi:10.1007/s11051-012-0880-y

2. Abbas K, Cydzik I, Del Torchio R, et al. Radiolabelling of TiO2 nanoparticles for radiotracer studies. *J Nanoparticle Res.* 2010;12(7):2435-2443. doi:10.1007/s11051-009-9806-8

3. Gibson N, Holzwarth U, Abbas K, et al. Radiolabelling of engineered nanoparticles for in vitro

and in vivo tracing applications using cyclotron accelerators. *Arch Toxicol*. 2011;85(7):751-773. doi:10.1007/s00204-011-0701-6

4. Rasmussen K, Mast J, De Temmerman P, Verleysen E, Waegeneers N, Van Steen F, Pizzolon J, De Temmerman L, Van Doren E, Jensen K, Birkedal R, Levin M, Nielsen S, Koponen I, Clausen P, Kofoed-Sørensen V, Kembouche Y, Thieriet N, Spalla O, Giuot C, Rousset D, MA. *Titanium Dioxide, NM-100, NM-101, NM-102, NM-103, NM-104, NM-105: Characterisation and Physico-Chemical Properties.*; 2014. doi:http://dx.doi.org/10.2788/79760

5. Robert Combes, Michael Balls, Rodger Curren, Michel Fischbach, Norbert Fusenig, David Kirkland, Claude Lasne, Joseph Landolph, Robert LeBoeuf, Hans Marquardt, Justin McCormick, Lutz Müller, Edgar Rivedal, Enrico Sabbioni, Noriho Tanaka, Paule Vasseur and HY. Cell Transformation Assays as Predictors of Human Carcinogenicity: The Report and Recommendations of ECVAM Workshop 39. *ATLA*. 1999;27, 5:745-767.

6. F Mazzotti, E Sabbioni, J Ponti, M Ghiani, S Fortaner GR. In Vitro Setting of Dose–effect Relationships of 32 Metal Compounds in the Balb/3T3 Cell Line, as a Basis for Predicting their Carcinogenic Potential. *ATLA*. 2002;(30, 2):209-217.

7. Ponti J, Ceriotti L, Munaro B, et al. Comparison of impedance-based sensors for cell adhesion monitoring and in vitro methods for detecting cytotoxicity induced by chemicals. *Altern Lab Anim*. 2006;34(5):515-525. doi:10.1177/026119290603400508

8. Tanaka N, Bohnenberger S, Kunkelmann T, et al. Prevalidation study of the BALB/c 3T3 cell transformation assay for assessment of carcinogenic potential of chemicals. *Mutat Res Toxicol Environ Mutagen*. 2012;744(1):20-29. doi:https://doi.org/10.1016/j.mrgentox.2011.12.008

9. Ponti J, Sabbioni E, Munaro B, et al. Genotoxicity and morphological transformation induced by cobalt nanoparticles and cobalt chloride: an in vitro study in Balb/3T3 mouse fibroblasts. *Mutagenesis*. 2009;24(5):439-445. doi:10.1093/mutage/gep027